New solar-biomass assisted thermophotovoltaic system and parametrical analysis

Shiquan Shan [a], Siqi Jia [a], Haojin Wu [a], Qi Zhang [a,c], Hongxun Hui [b], Zhijun Zhou [a,*]

[a] *State Key Laboratory of Clean Energy Utilization, Zhejiang University, Hangzhou 310027, China*
[b] *State Key Laboratory of Internet of Things for Smart City, University of Macau, Macau 999078, China*
[c] *Department of Mechanical Engineering, University College London, Torrington Place, London WC1E 7JE, UK*

ARTICLE INFO

ABSTRACT

This paper proposes a new technical route of solar-biomass assisted thermophotovoltaic (TPV) system for power generation which uses renewable fuel and contributes to carbon neutrality. Here, a thermophysics model is established for solar-biomass assisted TPV based on energy-balance principle. The effects of some key parameters on the new system performance are investigated, including concentrate ratio, emitter area, biomass fuels, etc. Besides, biomass fuel saving after adding solar energy is investigated. The results show that the solar-biomass assisted TPV system can not only increase the output power of photovoltaic cells by more than 10 kW/m^2 compared to biomass-driven TPV but also increase the electrical efficiency by nearly 10 percentage points. It is pointed out that improving the absorptance of solar absorber is the key for system optimization. Furthermore, the annual performance analysis shows that it also saves biomass fuel by up to 60% in one year. This study provides a reference for the design and application of renewable TPV technology.

1. Introduction

With the intensification of global energy and environmental issues, it is of strategic significance to achieve the goal of carbon neutrality on a global scale. Therefore, in terms of energy production technology, firstly, it is necessary to develop and utilize renewable resources such as solar energy (Su et al., 2017). Secondly, the development of new energy conversion technologies is a key measure to improve energy efficiency, which effectively guarantees the development and utilization of renewable energy.

Thermophotovoltaic (TPV) technology based on solar radiation energy is a potential new power generation technology. A typical TPV system consists of a heat source, emitter, filter, and photovoltaic cell. TPV also has many advantages such as low noise, light weight, high energy density, and flexible fuel adaptability (Bitnar et al., 2013). The solar thermo-photovoltaics (STPV) use solar radiation as heat source, a typical absorber which could harvest the solar energy and heat the emitter to a high temperature (Shan et al., 2022b). With the help of selective filter, the emitter can generate spectral radiation in a suitable waveband for photovoltaic cells. The theoretical thermodynamic efficiency of STPV can reach 85% (Shan et al., 2022a). Rephaeli et al. (2009) shows that STPV could achieve an efficiency of more than 50% theoretically based on

practical selective absorber and emitter, showing high application potential.

In recent years, researchers have continued to improve STPV, and the system performance has been developed. Nam et al. (2014) designed a planar STPV based on two-dimensional Ta photonic crystals and series filters, achieving a numerical efficiency of 10% at 1400 K. Ni et al. (2019) designed a STPV with a cavity-structured reflector in front of the absorber to recycle the infrared photons emitted from the absorber top surface, and the calculated efficiency is 17.4% at 50 concentration ratio. Chen et al. (2020) designed selective absorber and emitter based on tungsten spheres and SiO$_2$-coated substrates to match InGaAsSb photovoltaic cells. The numerical efficiency of the total STPV increases from 10.4% to 20.3% when the incident solar concentration ratio increases from 1 to 100. Recently, Chen et al. (2022b) designed a meta-material absorber and emitter to match a STPV system with molten salt energy storage. It is also (Shan et al., 2020b) pointed out that the key to improve the performance of STPV is the selective absorber or emitter based on micro/nano-structured materials, and scholars have also carried out related experiments. Lenert et al. (2014) obtained an experimentally efficiency of 3.2% using a photonic-crystal emitter. Ungaro et al. (2015) constructed STPV devices with GaSb cells and they used nanostructured tungsten as selective absorber/emitter, the obtained experimental efficiency reaches 6.2%. Recently, Bhatt and Gupta (2020) designed and

---

* Corresponding author.
E-mail addresses: zhouzj@zju.edu.cn, shiquan1204@zju.edu.cn (Z. Zhou).

Nomenclature

C	concentration ratio of solar collector
Cp	specific heat (J/(kg·K))
E	emissive power (W/m^2)
E_c	heat exchanger efficiency
E_g	PV cell bandgap (eV)
FF	fill factor
G	solar radiation intensity (W/m^2)
h	surface heat transfer coefficient W/(m^2·K) or enthalpy (kJ/kg)
J_{sc}	short-circuit current (A)
LHV	lower heating value (kJ/kg)
$\dot{m}$	mass flow rate (kg/s)
P	Power (kW)
r	solar-to-fuel input ratio
S	surface area (m^2)
T	temperature (K)
V_{oc}	open-circuit voltage (V)

Greek symbols

α	absorptance
η	efficiency
λ	transformation coefficient
ρ	reflectivity
ε	emittance
θ	energy-saving rate

Subscripts

ab	absorber
af	adiabatic flame temperature
air	air
cp	combustion product
em	emitter
egy	energy
el	electrical energy
f	flame or fuel
fuel	fuel
flt	filter
g	average flame temperature
out	outlet
sol	solar

fabricated an efficient STPV system which used two Si_3N_4 nanolayers with an intermediate W layer to form an emitter to match GaSb cell. It shows a system efficiency of 8.6% at 1670 K. Although the reported experimental efficiency of STPV is only about 10%, the recent experiment by LaPotin et al. (2022) determined that the TPV efficiency can reach 40%. This indicates the future development potential of TPV and STPV.

In practical application, there is supply discontinuity for solar energy; thus, STPV system should be developed and optimized. An effective solution is to combine energy storage technology. Seyf et al. (2016) proposed to use high-temperature silicon as thermal storage medium for STPV. Recently, Chen et al. (2022a, 2022b) proposed to use conventional molten salt energy storage mode for STPV power generation, and the related solar absorber and emitter are designed to achieve a system efficiency of 29% under medium temperature conditions. The problem of this technical route is the limited storage temperature, which limits the STPV efficiency. Another important technical route is the complementation of solar energy and fuel. This way could effectively improve the quality of solar energy since the fuel combustion has high temperature. Besides, Biomass fuel is an important renewable energy which is alternative to fossil fuels. The complementary of biomass fuels and solar energy can realize the clean energy production and conversion, which is of great significance to achieve carbon neutrality. There are many similar studies on thermal power cycle. Su et al. (2018) designed a solar-biogas assisted combined cooling heat and power system and found that there is economic advantage due to synthetic use of biogas and solar energy. Karapekmez et al. (2020) evaluated the effect of different biomass fuels on the performance of biomass-solar assisted power plant. The results show that the using of biomass could maintain considerable system efficiency and reduce the CO_2 emission effectively.

Therefore, it can be determined that the combination of biomass combustion and solar energy for TPV has a distinct application value. For TPV technology, most studies use gaseous fuels as power. For example, Li et al. (2009) proposed to use porous media as the heat source for micro-combustion TPV and use H_2 as fuel. Bani et al. (2018) further conducted experiments and numerical simulations for similar devices. Kang et al. (2017) used methane as the fuel, and experimentally verified that the use of selective filters could improve the performance of TPV with SiC emitter. The experimental study by Peng et al. (2020) demonstrated that H_2/C_3H_8/Air premixed combustion can be used for

micro-TPV, which can enhance flame stability and heat transfer performance. Based on fuel-driven TPV system, Shan et al. (2019a) proposed to use natural gas for oxy-fuel TPV system and use Brayton-Rankine combined cycle to form a combined system. On this basis, a cascade TPV system based on oxy-fuel combustion is proposed (Shan et al., 2019b). These designs are found to be effective in improving efficiency through optimization analysis. However, there are currently few TPV studies using biomass as fuel. Mustafa et al. (2015, 2016) innovatively used kerosene and vegetable cooking oil blend as fuel to conduct experimental research on TPV power generation. It can be seen that although much research on STPV and fuel-driven TPV has been done, there is few studies about solar-biomass assisted TPV system. It can be determined that the complement of solar energy and biomass fuel can achieve fully renewable energy-driven TPV, in line with the strategic goal of carbon neutrality. It has the advantages of increasing air preheating temperature, saving biomass fuel; overcoming solar instability; and improving solar energy conversion efficiency. Thus, it is necessary to start relevant fundamental research.

Against the above background, the reported studies mainly aimed at solar TPV or fuel-driven TPV. There is no report on the TPV driven by both solar energy and biomass fuel. Therefore, this work proposes a novel solar-biomass assisted TPV system and conducts parametrical analysis, which is innovative meaningful. The innovative work is as follows: (1) A new solar-biomass assisted TPV device is proposed, which achieves renewable energy driven and overcomes the disadvantage of solar instability. (2) A thermal-balance model is constructed for parametrical analysis of the new system. (3) The synergistic effects of key parameters on TPV system are investigated and the annual performance is analyzed to show system superiority. Based on the results, some recommendations for practical application are summarized.

2. Models and methods

2.1. Solar-biomass assisted TPV system

The concept of solar-biomass assisted TPV system is shown as schematic diagram in Fig. 1. It consists of solar collector system, biomass feeding device, combustion chamber, emitter, filter, and TPV cell. The air is heated by the concentrate solar radiation through solar collector system, and then enters the combustion chamber to assist the combustion of
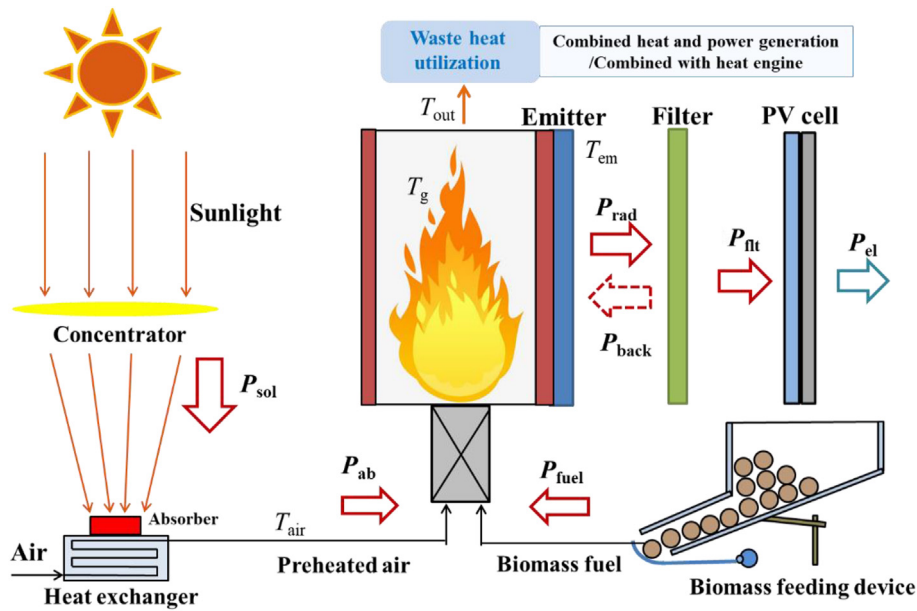
Fig. 1. Schematic diagram of solar-biomass assisted TPV system.

biomass fuel. The biomass is supplied to the combustion chamber by the feeding device. The emitter is set on the outer wall of the combustion chamber, which could generate radiative energy P_{rad}. Furthermore, the filter between emitter and PV cell could make the short-wavelength radiative energy P_{flt} pass, which matches the band gap of the PV cell. Besides, the long-waveband radiative energy P_{back} returns to the emitter to maintain its temperature, which could improve system efficiency. This TPV system uses biomass fuel and solar energy as dual heat source, and the high-temperature flue gas from the combustion chamber could enter the heat exchanger for further utilization.

2.2. Solar energy input model

In Fig. 1, solar collector system includes concentrator and receiver. Solar radiation is concentrated first and then absorbed by the receiver, which converts the solar energy into the thermal energy of input air. The thermal-balance equations of air preheating process of solar collector system are shown in Eqs (1)–(3). This study mainly considers the radiation heat transfer since it is the main form of heat transfer.

$$P_{ab} = P_{sol}\alpha\rho - \varepsilon S_1 \sigma\left(T_a^4 - T_0^4\right) \quad (1)$$

$$P_{ab} = \dot{m}_{air}(h_{air} - h_0) = \dot{m}_{air}\int_{T_0}^{T_{air}} Cp(air)dT \quad (2)$$

$$P_{sol} = CGS_1 \quad (3)$$

In equations, P_{sol} is the input solar power, P_{ab} is the absorbed power, and their unit is W. G is the unit solar radiation, and its value is set as 1000 W/m^2. C is concentrated ratio and S_1 is the absorber area, m^2. T_a, T_0 are the absorber surface temperature and ambient temperature, K. α is absorptance of the absorber, ε is the emissivity of the absorber, ρ is the reflectance of the concentrator, and is set as 0.9. These all constitute the optical loss of the solar collecting system. The heat transfer coefficient E_c between the working fluid and the surface of solar absorber can be expressed by Eq. (4).

$$E_c = \frac{T_{air} - T_0}{T_a - T_0} \quad (4)$$

It should be noted here that the established absorber model mainly reflects the basic physical laws. For the lower concentration ratio (below

100) the parabolic trough collector can be used, while the dish collector can be used for higher concentration ratio. Due to the large concentration range of the dish concentrator, a high-efficiency heat exchanger can be configured on it to achieve air preheating, so the practical application of the system can give priority to the dish collector.

2.3. Fuel and combustion model

In this study, the fuel input is typical biomass fuel and the input power is set as 10 kW. Here, $C_{a/12}H_{b/1}O_{c/16}N_{d/14}$ is used to represent 1 mol of dry fuel and a, b, c and d is the amount of each element in mass percentage. The air is used as a combustion-supporting gas. The chemical reaction of combustion is:

$$C_{a/12}H_{b/1}O_{c/16}N_{d/14} + fH_2O + k(O_2 + 3.76N_2) \rightarrow x_1CO_2 + x_2H_2O + x_3N_2 + x_4O_2$$
$$+ \text{Ash} \quad (5)$$
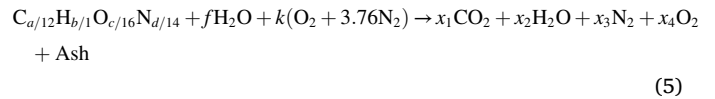
where, the coefficient f represents the moles of water per mole of dry fuel, k is exceeding air ratio and is set to 1.1 in this study (Shan et al., 2019b). It is assumed that ashes heat capacity for any kind of biomass was 0.77 kJ/(kg·K) according to the reference (Durante et al., 2017). The sulphur in the considered biomasses is less than 0.1%, and thus it is not considered in computation (Durante et al., 2017). Numerical computations are performed for different biomasses, always considering an input power of 10 kW and 25% moisture on dry basis (mass content). Moreover, two biomass fuels of pine wood and rice husk are considered in this study and their ultimate analysis is presented in Table 1 (Durante et al., 2017). It is mainly because the two biomass fuels are widespread in China. In fact, the calorific value of biomass fuel is close to that of lignite, and its water content of 25% is close to that of high-volatile lignite (Shan et al., 2020a). The calculation method of flue gas enthalpy and adiabatic temperature of combustion is based on literature (Turns et al., 2011).

Table 1
Ultimate analysis of different biomass fuels.

	C (%)	H (%)	O (%)	N (%)	Ash (%)	LHV (kJ/kg)
Pine wood	49.3	6.0	44.4	<0.01	0.3	18681
Rice husk	41.0	5.9	35.9	0.4	18.9	14800

The thermal-balance calculation of the TPV system is consistent with our previous research (Shan et al., 2019b); thus, only a brief introduction is given here. According to the energy conservation, there are:

$$P_{in} = P_{fuel} + P_{sol} \tag{6}$$

where fuel input energy is:

$$P_{in} = \dot{m}_{fuel} LHV \tag{7}$$

The ratio r of solar energy to fuel input can be expressed by the following equation:

$$r = \frac{P_{sol}}{P_{fuel}} \tag{8}$$

Here the input solar energy refers to the P_{sol} projected into the concentrator system, represented by Eq. (3). The adiabatic flame temperature can be expressed by Eq. (9), and the enthalpy of combustion flue gas is defined according to the reference (Turns et al., 2011).

$$\dot{m}_{cp}(h_{af} - h_0) = \dot{m}_{cp} \int_{T_0}^{T_{af}} Cp(cp)dt = P_{fuel} + P_{ab} \tag{9}$$

The thermal balance between the high-temperature flue gas inside the combustion chamber and the emitter radiation is shown below and it is considered that the combustion chamber wall temperature T_w is approximately the same as the emitter wall temperature T_{em}.

$$P_{flt} = \varepsilon_{sys}\sigma(T_g^4 - T_w^4)S_2 + h(T_g - T_w)S_2 \tag{10}$$

$$P_{flt} = \dot{m}_{cp} \int_{T_{out}}^{T_{af}} Cp(cp)dT \tag{11}$$

$$T_w = T_{em} \tag{12}$$

where h is the convective heat transfer coefficient between flue gas and the wall and is set as 180 W/m^2 K to make the model more in line with the actual physical process (Shan et al., 2019b).

In addition, the radiative energy passing through the filter can be defined as follows:

$$P_{flt} = S_2 \int_0^{\lambda_c} \varepsilon_{em}(\lambda)E_b(\lambda, T_{em})d\lambda \tag{13}$$

The emissivity ε_{em} of the emitter is set to 0.9, and λ_c is the cut-off wavelength of the filter corresponding to the PV cell. The calculations of system emissivity ε_{sys} and flame gas temperature T_g are shown in Appendix. According to the constructed model, T_{out} is assumed and the iteration is conducted then to obtained T_{em}, T_g, P_{rad} and P_{flt}. The power generation P_{el} could further be obtained through P_{rad}; the thermal balance iteration flow chart of the TPV system is similar to our previous paper (Shan et al., 2019b), which is implemented by Fortran code and we also attached it in Appendix.

Moreover, the spectral radiation efficiency is defined to evaluate the radiative energy proportion generated by the emitter.

$$\eta_{flt} = \frac{P_{flt}}{P_{sol} + P_{fuel}} \tag{14}$$

2.4. TPV cell model

In this study, two photovoltaic cells, Si and GaSb (Shoaei et al., 2016), with band gaps of 1.1 eV and 0.72 eV are investigated respectively. Therefore, the cut-off wavelengths of the filter corresponding to these two photovoltaic cells were 1.1 μm and 1.8 μm, respectively. In this study, the TPV cell is completely parallel to the emitter, so the area of the cell is the same as that of the emitter, namely S_2. The TPV cell model is based on Shan et al. (2019b).

The output power P_{el} of the photovoltaic cell can be defined as:

$$P_{el} = V_{oc} \cdot FF \cdot J_{sc} \tag{15}$$

The short-circuit current J_{sc} is calculated according to Eq. (16):

$$J_{sc} = S_2 \int_{\lambda_0}^{\lambda_c} \frac{q_0\lambda}{hc} EQE(\lambda)\varepsilon_{em}(\lambda)E_b(\lambda, T_{em})d\lambda \tag{16}$$

where EQE is the external quantum efficiency, q_0 is the elementary charge, h is the Planck constant, and c is the speed of light.

The open circuit voltage can be calculated as follows:

$$V_{oc} = \frac{\Gamma kT_c}{q_0} ln\left(\frac{J_{sc}}{J_0} + 1\right) \tag{17}$$

where k is the Boltzmann constant; Γ is the diode ideality factor, which takes the value of 1 in this study; T_c is the surface temperature of the PV cell (constant 300 K); J_0 is the diode saturation current of the PV cell, which can be calculated using the following empirical equation.

$$J_0 = 1.5 \times 10^5 \exp\left(\frac{-E_g}{kT_c}\right) \tag{18}$$

The filling factor is calculated using the following equation, and the correction factor β is taken to be 0.96.

$$FF = \beta\frac{\nu - ln(\nu + 0.71)}{\nu + 1} \tag{19}$$

where ν is the normalized open-circuit voltage, which can be defined as follows:

$$\nu = \frac{q_0}{kT_c}V_{oc} \tag{20}$$

The photovoltaic cell efficiency η_{cell} is defined as follows:

$$\eta_{cell} = \frac{P_{el}}{P_{flt}} \tag{21}$$

2.5. System efficiency

According to the models, the power generation efficiency of the system is defined as follows:

$$\eta_{sys} = \frac{P_{el}}{P_{sol} + P_{fuel}} \tag{22}$$

In this paper, in order to investigate the energy-saving effect of the solar-fuel assisted TPV system, the efficiency $\eta_{sys,n}$ of the TPV system using fuel alone (non-complementary) is specially calculated. The fuel consumption $P_{fuel,n}$ of the non-complementary TPV system can be calculated from $\eta_{sys,n}$ and the electric energy produced P_{el} under specific operating conditions; therefore, the energy saving rate of the solar-fuel assisted TPV system is defined as follows:

$$\theta_{egy} = \frac{P_{fuel,n} - (P_{sol} + P_{fuel})}{P_{fuel,n}} \tag{23}$$

Moreover, the fuel saving rate of a solar-fuel assisted TPV system is defined as follows:

$$\theta_{fuel} = \frac{P_{fuel,n} - P_{fuel}}{P_{fuel,n}} \tag{24}$$

In this paper, the energy saving effect of the system can be evaluated by θ_{egy} and θ_{fuel}. Based on the above-mentioned physical models, the Fortran code is used for programming in this study and the whole simulation flow chart is shown in Appendix.

It should be noted that the TPV model, combustion chamber model and solar concentrating system model used in this paper were all established based on the previous research and experimental results. Based on the radiation calculation theory of solid fuel boilers, this paper innovatively established a thermal-balance model for biomass fuel combustion. Based on these key physical models, a thermophysical analysis model of the solar-biomass assisted TPV system is established for performance analysis. Therefore, previous related researches (Shan et al., 2019b, Shan et al., 2020b) just illustrate the effectiveness of these sub-models, providing support for this study. In addition, this paper mainly focuses on the macro law and coupling effects of key parameters on the system, so the range of investigating parameter is wide. In this study, the influence of a series of parameters including concentration ratio is mainly considered. Some main concerned parameters of the system are listed in Table 2.

3. Results and discussion

3.1. Effect of biomass fuel and PV cell

At first, we investigate two biomass fuels of pine wood (Fuel-1) and rice husk (Fuel-2), two PV cells of Si and GaSb, with air condition of 21% O_2/N_2, to select the representative case for this study. Here, the basic case is set as follows: the absorptance α is 0.85, emittance of absorber ε_a is 0.2, and the heat transfer coefficient E_c is 0.8. At first, three key cases for different concentration ratio, receiver area and emitter area is used to investigate the effect of biomass fuel and PV cell based on preliminary calculations: (1) $C = 400$, $S_1 = 0.02$ m^2, $S_2 = 0.3$ m^2; (2) $C = 500$, $S_1 = 0.025$ m^2, $S_2 = 0.35$ m^2; (3) $C = 600$, $S_1 = 0.03$ m^2, $S_2 = 0.4$ m^2. Moreover, the control variable comparison method is used here. The case of Si cell matching Fuel-1 is used as the basic reference condition. A more representative fuel is determined by comparing it with the case of Si cell matching Fuel-2; and a more representative PV cell is determined by comparing it with the case of GaSb cell matching Fuel-1.

Fig. 2 shows that under typical cases, the electrical efficiency of TPV system η_{sys} for pine wood is higher than that for rice husk; this is mainly due to the higher emitter temperature T_{em} for pine wood fuel as shown in Fig. 2(b). The higher T_{em} causes much more spectral radiation shifts to short-wavelength direction; therefore, the spectral efficiency η_{flt} is higher for pine wood as shown in Fig. 2(c). Moreover, the cell efficiency η_{cell} are similar for different fuels. Fig. 2 also shows that η_{sys} of TPV system with Si cell is about 4~5 percentage points higher than that of GaSb cell. For this result, it should be noted that the filter for Si cell has shorter cut-off wavelength. Thus, there is more spectral radiation not suitable for cell returned to the combustion chamber by the filter for the TPV device with Si cell, and the P_{flt} is less. This maintains the emitter temperature T_{em}. As shown in Fig. 2(b), the T_{em} of TPV device using Si cell is always higher than that using GaSb cell under three cases. The high-temperature condition makes the spectrum peak shift to the short wavelength direction; this is the reason for the higher efficiency of Si cells. As shown in Fig. 2(d), the efficiency of Si cells is about 13 percentage points higher than that of GaSb cells. Therefore, even under the conditions of low η_{flt}

(Fig. 2(c)), the η_{sys} of TPV systems using Si cells is higher than that using GaSb cells. Since the Si cell has lower cost, it is more suitable for solar-fuel assisted TPV system. Based on these results, the following analysis will focus on pine wood fuel and Si cell.

3.2. Effect of concentrate ratio

This section mainly investigated the influence of solar concentration ratio. Fig. 3 shows the effect of the concentration ratio on the air preheating temperature T_{air} under basic cases ($\alpha = 0.85$, $\varepsilon_a = 0.2$, $E_c = 0.8$, $S_2 = 0.4$ m^2) with different absorber areas S_1, the Si cell case is selected. Fig. 3(a) shows that when the absorber area S_1 is 0.01 m^2 and 0.02 m^2, with the continuous increase of the concentration ratio, the system P_{el} increases almost linearly, which increases by 3.4 kW and 6.74 kW, and the power density increased by 8.51 kW/m^2 and 16.86 kW/m^2, respectively. When C is 1000 and 600, the power density of the combined system can be increased by 18.72 kW/m^2 and 11.30 kW/m^2, respectively compared to the only biomass combustion condition (5.35 kW/m^2). Moreover, the η_{sys} of TPV system increased by 6 and 5.7 percent points, respectively. The increase of the concentration ratio causes the increase of the emitter temperature, which improves η_{cell} of the photovoltaic cell. Thus, the TPV system efficiency increases. It can be seen from Fig. 3(a) that when C is greater than 500, the increasing trend of η_{sys} slows down. This is because P_{sol_in} increases greatly with the concentration ratio C. At the same time, the increase trend of η_{cell} versus C is reduced as shown in Fig. 3(b), which also directly affects the system efficiency trend versus C as in Fig. 3(a). It can be seen that when the concentration ratio is 600, the growth rates of the η_{sys} and η_{cell} begin to decrease significantly. Therefore, it is no need to select an excessively large emitter area and concentration ratio. In addition, it should be noted that when designing the concentration ratio and the absorber area of solar-biomass assisted TPV system in practical engineering, special attention should also be paid to the upper limit of the air preheating temperature, otherwise the pipeline will be damaged by the working fluid (Quero et al., 2014). If the preheating temperature is higher, some safety hazards during the combustion process may also arise. To sum up, the concentrating ratio suitable for this system can be selected between 400 and 500, and the absorber area can be selected as 0.02 m^2.

In this section, we further investigate the effect of the absorptance α and heat transfer coefficient E_c of the solar absorber on the system performance under different concentration ratio. The basic case is set as $S_1 = 0.02$ m^2, $S_2 = 0.4$ m^2. It can be seen from Fig. 4 that when the absorption rate α changes from 0.6 to 0.9, the air preheating temperature increases from 525.6 K to 635.2 K (a variation of about 110 K) for $C = 600$, and the system efficiency increases from 24.2% to 31.5%, showing an obvious trend. Moreover, the air preheating temperature increases from 375.9 K to 413.6 K (a variation of about 40 K) for $C = 200$, and the system efficiency increases from 22.8% to 26.6%. It shows that increasing the optical absorptance can greatly improve the performance of the absorber, and the larger the concentration ratio, the more significant the impact of the absorptance parameter on the system performance. On the other hand, as can be seen from Fig. 5, when α is set to 0.75, the T_{air} increases from 579.5 K to 581.3 K (a variation of about 3 K) for $C = 600$ with the increase of E_c from 0.6 to 1, while the system efficiency increases from 27.8% to 27.9%, showing a slight change. Besides, the T_{air} increases from 394.6 K to 394.8 K (a variation of about 1 K) for $C = 200$ with the increase of E_c from 0.6 to 1, while the system efficiency is about 24.73% with a little change less than 0.1%. It shows that the heat transfer coefficient of the absorber has little influence on the performance under thermal-balance condition regardless of any concentration ratio. Therefore, it can be concluded that for solar absorber, it is more significant to improve the absorptance α than to optimize the heat exchanger efficiency E_c. In recent years, selective coating absorbing materials can achieve a high absorptance more than 90% (Li et al., 2015), which should be investigated in the future.

Table 2
Main concerned parameters in the system.

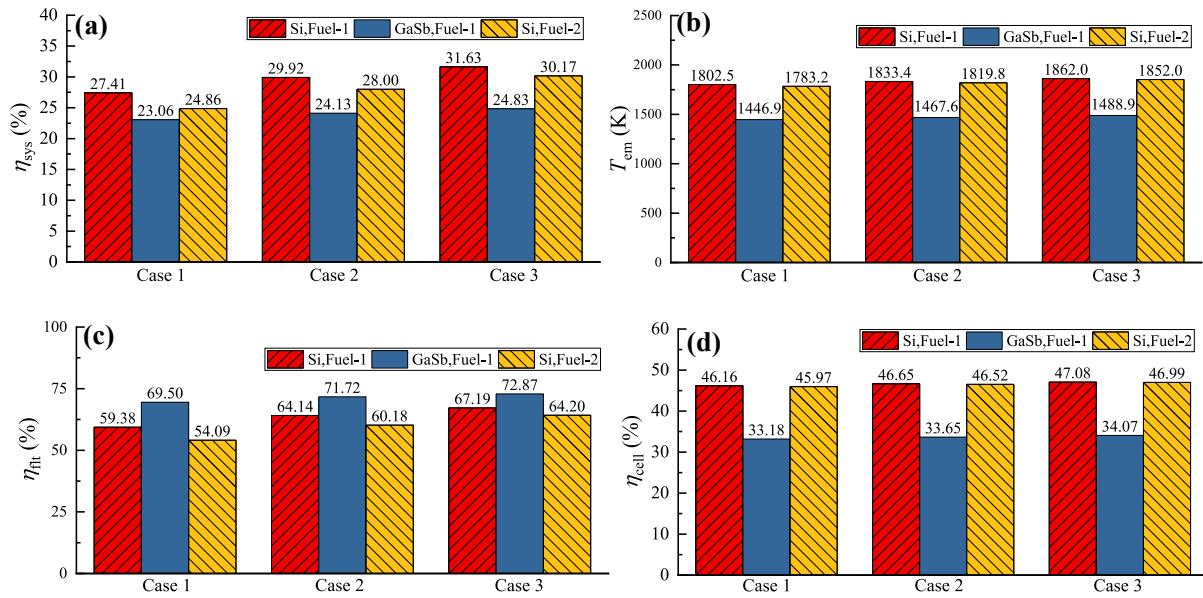| Parameters	Symbol	Unit
Concentration ratio	C	
Heat exchanger efficiency	E_c	
Absorber surface area	S_1	m^2
Emitter or PVcell area	S_2	m^2
Absorptance of absorber	α	
Emittance of absorber	ε	
Temperature of absorber	T_a	K
Temperature of emitter	T_{em}	K
solar-to-fuel input ratio	r	
System efficiency	η_{sys}	%

Fig. 2. Effect of different biomass and PV cell on system: (a) TPV efficiency; (b) emitter temperature; (c) spectral radiation efficiency; (d) cell efficiency.
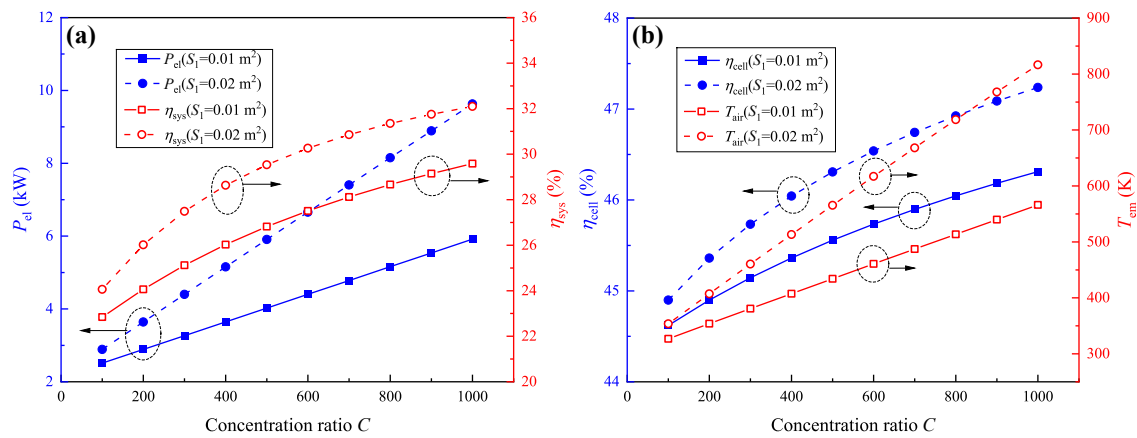

Fig. 3. Effect of the concentration ratio on the power generation performance under different absorber areas: (a) the PV cell output power and system efficiency; (b) the PV cell efficiency.
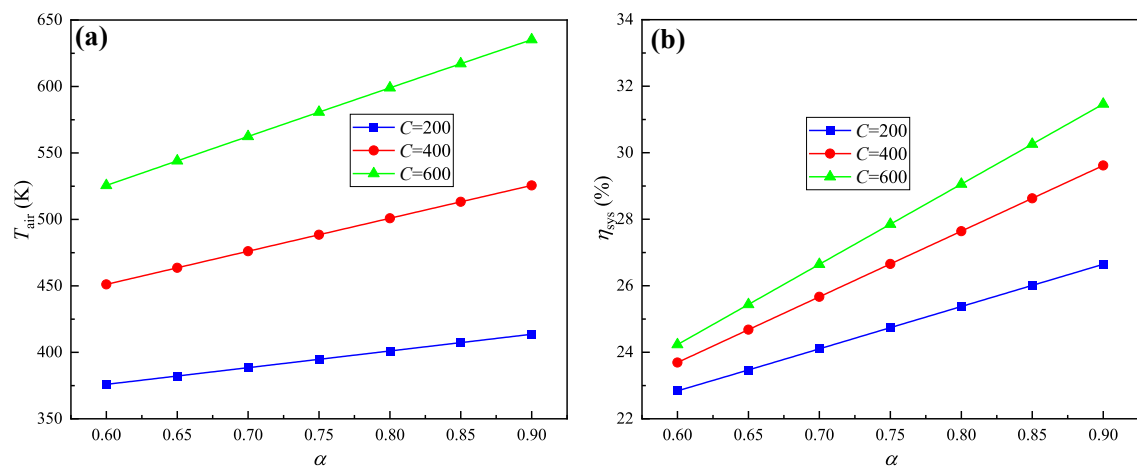

Fig. 4. Effects of radiation absorptance of solar absorber on system performance: (a) preheated air temperature T_{air}; (b) system efficiency η_{sys}.
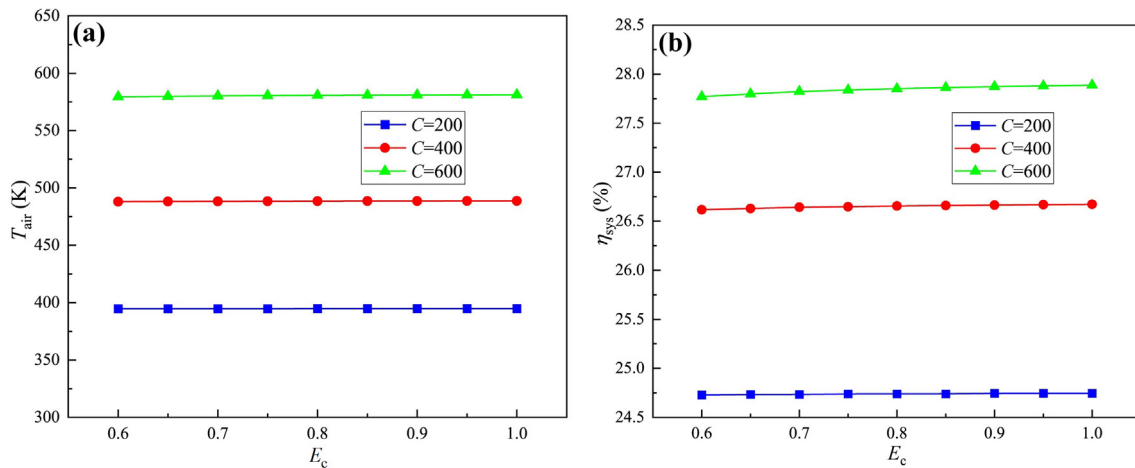
Fig. 5. Effects of heat transfer coefficient of solar absorber on system performance: (a) preheated air temperature T_{air}; (b) system efficiency η_{sys}.
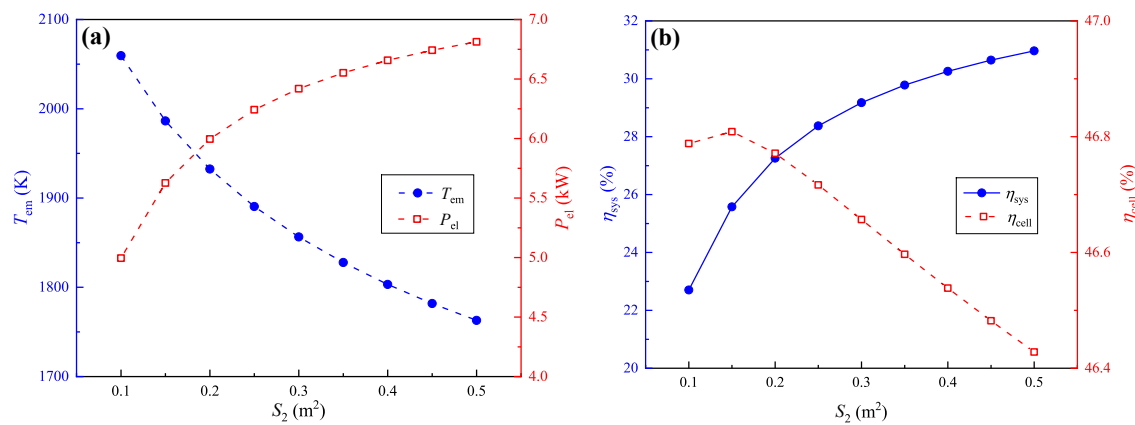
Fig. 6. Effect of emitter areas on solar-fuel assisted TPV system: (a) output power and emitter temperature; (b) system efficiency and cell efficiency.

3.3. Effect of emitter area

In the solar-biomass assisted TPV system, the determination of the emitter area S_2 is also particularly important. This is because S_2 determines thermal radiation from the emitter, which directly affects the performance such as the output power and system efficiency. Fig. 6 reflects the effect of emitter area ($C = 600$, $S_1 = 0.02\,\mathrm{m^2}$). Here, the emitter area is the independent variable. It can be seen from Fig. 6(a) that as the S_2 increases from 0.1 $\mathrm{m^2}$ to 0.5 $\mathrm{m^2}$, the output power increases from 5.0 kW to 6.81 kW. This indicates that the radiative power is proportional to the emitter area. In addition, it also shows that the T_{em} gradually decreases from 2059 to 1763 K, which is due to the thermal-balance calculation results after the area increases. Due to the decrease in temperature, the output power increases faster first and then slower, showing a similar trend. It should be noted that Fig. 6(a) shows that when S_2 reaches 0.4 $\mathrm{m^2}$ or more, the emitter temperature is about 1700~1800 K. In this study, since both solar energy and biomass combustion is used for input, which forms a preheating process, theoretically higher combustion temperatures can be achieved. In previous literatures (Chen et al., 2021; Collazo et al., 2012) the maximum temperature of the biomass combustion furnace can reach more than 1700 K, which shows that it is more reasonable to choose a larger emitter area S_2 of more than 0.4 $\mathrm{m^2}$. Besides, Fig. 6(b) indicates that the η_{sys} increases from the initial 22.7% ~31% with the emitter area, showing a trend of increase fast first and slow then. It can be found that this is consistent with the power results in Fig. 6(a). This is mainly due to the dual effects of emitter area and temperature. In addition, the cell efficiency shows a decrease trend from

about 46.8% to 46.4%, which is mainly due to the decrease in T_{em}. It should be noted that η_{cell} here refers to cell efficiency, and the results are similar to the data reported by Qiu et al. (2006). As a parameter analysis result, Fig. 6 shows the relationship between emitter area and system efficiency, and a larger emitter area has practical significance. In addition, the larger the emitter area, the less obvious the improvement of system efficiency due to the reduction of T_{em}. Therefore, it is not possible to blindly increase the emitter area to increase the output power and system efficiency of the photovoltaic cell in practical applications.

3.4. Energy-saving effect with solar and fuel complementary

The energy-saving effect of the solar-biomass assisted TPV system is also investigated in this study for the basic case ($S_1 = 0.02$ $\mathrm{m^2}$ and $S_2 = 0.4$ $\mathrm{m^2}$). Fig. 7(a) shows that as the ratio of solar energy to biomass fuel input r increases from 0 to 2, η_{sys} increases from 24.1% to 32.1% with an increase of about 8 percentage points. It should be noted here that the data of $r = 0$ in Fig. 7(a) means that there is no solar energy input. Through calculating the biomass-driven TPV model, the system efficiency is 21.4%. Therefore, it can be seen from Fig. 7(a) that any solar-biomass assisted case has higher efficiency than the only biomass-driven case. This parametric study mainly considers the basic law in a wide range of r from 0 to 2, including the combustion of biomass fuel alone and the large-scale complementation of solar energy. Therefore, this indicates that the addition of solar energy could improve the energy conversion efficiency, which is mainly because the introduction of solar energy increases the preheating temperature T_{air}, which increases the
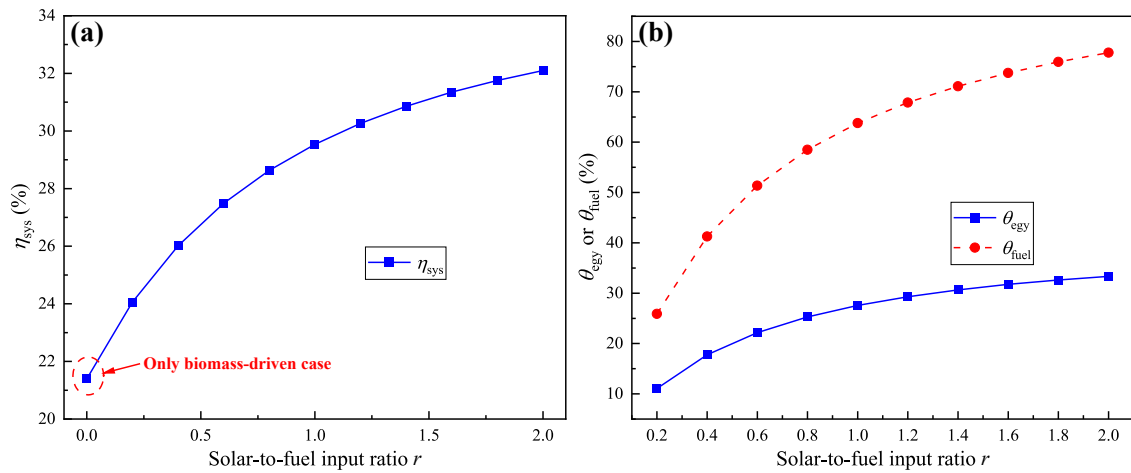
Fig. 7. Effect of solar-to-fuel input ratio on the system performance: (a) system efficiency; (b) energy and fuel savings characteristics.

combustion temperature T_g, thereby increasing the emitter temperature T_{em} and improving the TPV system efficiency. Moreover, when the ratio r is greater than 1, the increase rate of the system efficiency slows down. Fig. 7(b) shows that when the input ratio r increases from 0.2 to 2, the energy-saving rate θ_{egy} of the system increases from 11.07% to 33.34%, which is the result of the increase in system efficiency. The fuel-saving rate θ_{fuel} increases from 25.89% to 77.78%, which results from the dual effect of the system efficiency increase and the solar energy complementary. This fully indicates the advantages of introducing solar energy into biomass-driven TPV. However, if too much solar radiation is introduced to preheat the air, it will also bring higher costs and safety hazards to the system, so the ratio of solar energy to fuel input can be controlled at about 1, which also meets the definition of a solar-biomass assisted TPV system.

3.5. Annual performance results

The solar radiation calculation model reported by Gholamalizadeh et al. (2017) is used in this study, and the latitude and longitude of Hangzhou, China are taken as an example. The efficiency and energy saving performance in a typical day of each month are calculated. Here, the basic case ($C = 600$, $S_1 = 0.02$, $S_2 = 0.4$ m^2, $P_{in} = 10$ kW) is selected. Here, we only count data in solar irradiation time. The model in this study draws on the dual-axis tracking system, which can capture the solar energy to the greatest extent, so the absolute difference among the daily irradiance is not large (Gholamalizadeh et al., 2017). Fig. 8 shows the
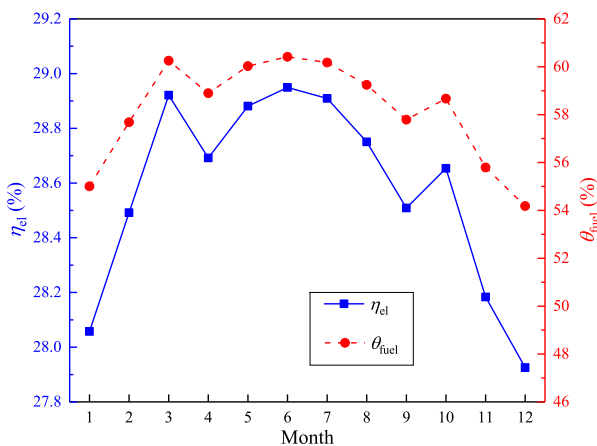
Table 3
Annual performance results of solar-fuel assisted TPV system.

Annual performance	Fuel input (kWh)	Fuel input of non-assisted system (kWh)	Solar-to-fuel input ratio	Power generation efficiency	Fuel saving rate
Value	43810	105261.7	0.7970	28.61%	58.38%

power generation efficiency η_{el} and fuel saving rate θ_{fuel} of system for typical days in each month. It can be seen that, the η_{el} of system is around 28~29%, which is higher in summer than in winter. This is mainly because the irradiance obtained by the system is smaller in winter, so the solar-to-fuel input ratio r is lower (about 0.48), while the r in summer is about 0.59. According to the analysis of this paper, the large r achieves the increase of flame temperature of TPV system, thereby improving the system efficiency. Further, the system overall performance within one year is calculated and the results are shown in Table 3. It can be seen that if the non-assisted system is used, the annual fuel consumption is about 60,000 kWh, and the annual fuel saving of the assisted system achieves 58.38%. The annual electrical efficiency of the system reaches 28.61%, which is about 6 percentage points higher than the non-assisted system (21.40%). Therefore, the new system has practical potential and can produce considerable benefits.

3.6. Application prospect analysis

The thermo-photovoltaic device has the advantages of small size, no rotating parts, direct current generation, high efficiency, easy for waste heat recovery and so on. Therefore, the future application of the solar-biomass assisted TPV conversion system proposed in this paper will mainly consider the following scenarios.

(1) Distributed energy cogeneration supply, which can be applied to the combined heating and power supply of buildings and factories. In addition, it is especially suitable for the borderland and remote area, plateau section and other areas where the grid power supply is lacking, where solar energy and biomass resources are rich, and cogeneration can be carried out in small areas.

(2) The TPV system has high efficiency and good integration, so it can be combined with thermal power cycles such as Rankine cycle and Brayton cycle, which can be used for distributed thermal power generation.

(3) The complementation between solar energy and biomass can be flexible. Future application can consider solar-driven biomass gasification for generation of gas fuel, which is then used for TPV system.

Fig. 8. System electrical efficiency and fuel saving rate in a typical day of each month.

4. Conclusions

This study innovatively proposes a design concept of solar-biomass assisted TPV system for the aim of carbon neutral, and the effect of some parameters on the system performance is analyzed. This study provides a reference for the design of STPV, and its main conclusions are as follows.

(1) The system performance is better when pine wood fuel and Si cell is used. The electrical efficiency is around 4~5 percentage points higher than that of GaSb cell. This is because the emitter temperature after thermal balance is higher for Si cell and pine wood fuel. In addition, since Si cell has lower cost, it has practical value in application.

(2) With the increase of solar concentration ratio, the output power density can increase by nearly 16 kW/m^2 and the electrical efficiency of the TPV system can increase by nearly 6 percent points for the system with Si cell. Considering the economic cost and system safety, the concentrating ratio suitable for solar-fuel assisted TPV system can be selected to be around 500~600; the solar absorber area should not be too large to ensure a reasonable solar-to-fuel input ratio.

(3) When the absorptance α of the solar absorber increases from 0.6 to 0.9, the system efficiency can be increase by about 7 percentage points, and the increase effect is more obvious. Compared with the heat exchanger efficiency E_c, it is more significant to improve the absorptance of solar absorber in system optimization.

(4) The emitter area of TPV is the main factor affecting the output power and efficiency of the system. At the same time, as the emitter area increases, the emitter temperature decreases based on thermal balance, so the increasing rate of the output power decreases gradually. Therefore, in the solar-fuel assisted TPV system, the selection of emitter area is not as large as possible.

(5) The solar-fuel assisted TPV system has a significant energy-saving effect. When the solar-to-fuel input ratio increases from 0.2 to 2, the system energy-saving ratio increases from 11.07% to 33.34%. At the same time, the system biomass fuel-saving ratio increases from 25.89% to 77.78%. The solar-biomass assisted TPV system can achieve an annual fuel saving efficiency of 50.82%. The ratio of solar energy to biomass fuel input should be controlled at about 1 since the introduction of too much solar radiation to preheat the air will also bring safety hazards to the system.

Declaration of competing interest

The authors declare that they have no known competing financial interests or personal relationships that could have appeared to influence the work reported in this paper.

Acknowledgements

Appendix

(1) Supplementary for the model of combustion chamber

The appendix mainly gives more introduction on the combustion chamber calculation. In Eq. (10), the system emissivity ε_{sys} could calculated by:

$$\varepsilon_{\mathrm{sys}} = \frac{1}{\frac{1}{\varepsilon_f} + \frac{1}{\varepsilon_w} - 1} \tag{A1}$$

where the flame emissivity ε_f is the combination of gas radiation and particle radiation (Rong et al., 1997). Its expression is as follows:

$$\varepsilon_f = 1 - e^{-\kappa ps} \tag{A2}$$

In Eq. (A2), s is the path-length: $s = 3.6\,V/F$, V is furnace volume and F is furnace area; p is pressure and set to 0.1 MPa; κ is the absorption coefficient of flame radiation (Rong et al., 1997). For solid fuels combustion, both gas and particle radiations need to be considered.

$$\kappa = \kappa_g r_g + \kappa_{ah}\mu_{ah} + \kappa_c x_1 x_2 \tag{A3}$$

where κ_g is the gas extinction coefficient; it is calculated by the WSGG model (Shan et al., 2017) and its WSGG model parameters in Shan et al. (2018) are used in this study. The parameter selection for Eq. (A3) can refer to Shan et al. (2020a) and Rong et al. (1997). r_g is gas volume fraction; κ_{ah} is the fly ash extinction coefficient which could be estimated by $\kappa_{ah} = 55900/\sqrt[3]{T_g^2 d_h^2}$, and d_{ah} is ash particle diameter and is set as 13 μm; μ_{ah} is fly ash concentration; κ_c is the char extinction coefficient and is set as 10 (m·MPa)$^{-1}$; $x_1 = 0.5$ for biomass solid fuel; $x_2 = 0.1$ for pulverized fuel furnace.
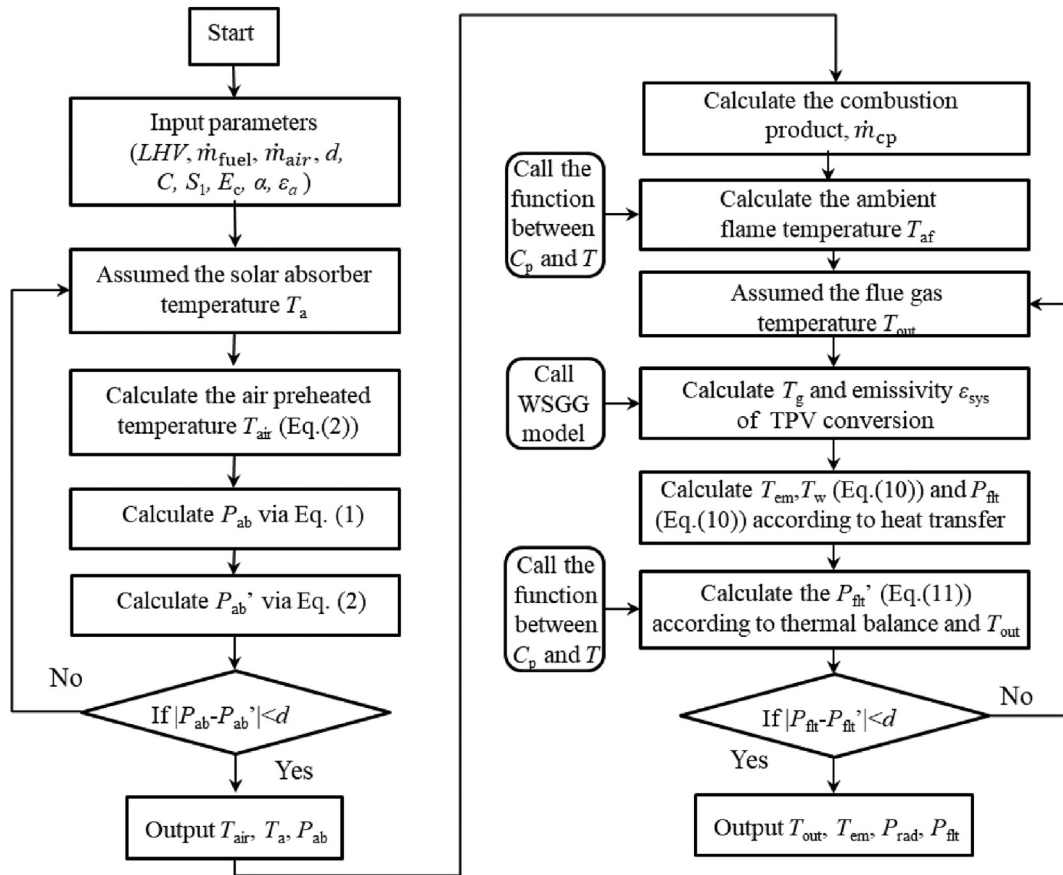
Fig. A1. Flow chart of thermal-balance calculation for solar-fuel assisted TPV device.

In addition, the calculation of flame temperature could refer to Shan et al. (2019b) and Zhang et al. (2016). The relationship between the average furnace gas temperature T_{fla} and the outlet flue gas temperature T_{F2} can be expressed as follows:

$$T_g^4 = R T_{out}^4 \tag{A3}$$

where the relationship between the coefficient R and the adiabatic flame temperature T_a is according to Zhang et al. (2016):

$$R = \frac{3}{\left(T_{out}/T_{af}\right)^3 + \left(T_{out}/T_{af}\right)^2 + T_{out}/T_{af}} \tag{A4}$$

The flow chart for thermal-balance calculation of solar-biomass assisted TPV is shown in Fig. A1.

(2) Model Validation

We first verify the solar absorber model in this study. The absorption efficiency is compared with several typical absorbers that have been published. The absorption efficiency calculation refers to Shan et al. (2022b). When $C = 600$, the absorption efficiency of the absorber in this paper is 85%, while that of the absorber reported in Rinnerbauer et al. (2014) is 82.73% (Ta photonic crystal), and is 89.90% (W/WAlN/WAlON/Al$_2$O$_3$) in the study of Dan et al. (2019). The solar absorber results are similar to that published in the existing references. Because this study is about model performance analysis, such a parameter setting is also reasonable.

It should be noted that when calculating the absorption performance of the solar absorber via Eq. (1), the thermal balance of radiation heat transfer is mainly considered. The purpose is to simplify the model and highlight the key laws. This study considers the higher concentration, so the absorption efficiency is high (over 80%), and the effect of convective heat transfer is theoretically low. The thermal efficiency of the absorber can be written as follows:

$$\eta_{ab} = \left[P_{sol}\alpha\rho - \varepsilon S_1 \sigma \left(T_a^4 - T_0^4\right)\right] / (P_{sol}\rho) \tag{A5}$$

If convective heat transfer is considered, the thermal efficiency of the absorber can be written as follows:

$$\eta_{ab} = \left[P_{sol}\alpha\rho - \varepsilon S_1 \sigma \left(T_a^4 - T_0^4\right) - h(T_a - T_0)\right] / (P_{sol}\rho) \tag{A6}$$

According to the heat transfer book (Bergman et al., 2011), the air convective heat transfer coefficient h can be taken as 5 W/m^2·K. when C is 600, the thermal efficiency of the absorber at different temperatures is calculated, as shown in Fig. A2. It can be seen that under practical temperature conditions, whether convective loss is considered will have minimal impact on system performance (no more than 0.5%). Therefore, it shows that using the radiation heat transfer model in Eq. (1) can complete this study to analyze the system law.

Furthermore, the fuel-driven TPV model is verified. Here, a porous medium TPV combustor with a wall length of 20 mm and a diameter of 8 mm designed by Peng et al. (2020) is used for investigated. In their study, premixed H$_2$/C$_3$H$_8$/air flow is input and the selected equivalence ratio of fuel/air is 1.0. Therefore, it is regarded as a cylindrical burner, the average temperature of the emitter T_2 and the average temperature of the combustion flame T_g are calculated through the thermal-balance model of this paper. The results show that the calculated T_2 is 978.8 K, which is in the range of the experimental results between 908.7 K and 1085.4 K. Moreover, the calculated T_g is 1101.2 K and it is slightly higher than the experimental wall temperature, which conforms to the actual physical process. Thus, the verification results indicate that the thermal-balance model is valuable for reference.
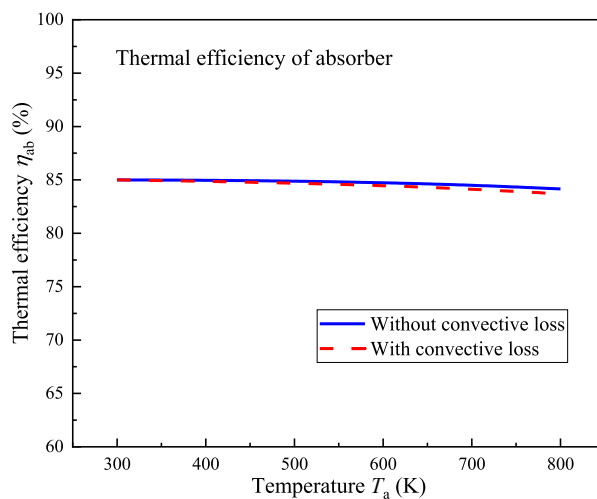

Fig. A2. Calculated thermal efficiency of absorber at different temperatures.

References

Bani, S., Pan, J., Tang, A., et al., 2018. Micro combustion in a porous media for thermophotovoltaic power generation. Appl. Therm. Eng. 129, 596–605.

Bergman, T.L., Bergman, T.L., Incropera, F.P., et al., 2011. Fundamentals of Heat and Mass Transfer. John Wiley & Sons.

Bhatt, R., Gupta, M., 2020. Design and validation of a high-efficiency planar solar thermophotovoltaic system using a spectrally selective emitter. Opt Express 28 (15), 21869–21890.

Bitnar, B., Durisch, W., Holzner, R., 2013. Thermophotovoltaics on the move to applications. Appl. Energy 105, 430–438.

Chen, M., Yan, H., Zhou, P., et al., 2020. Performance analysis of solar thermophotovoltaic system with selective absorber/emitter. J. Quant. Spectrosc. Radiat. Transf. 253, 107163.

Chen, R., Yue, H.H., Yue, R., et al., 2021. Numerical simulation of combustion in a biomass briquette chain boiler. Biomass Conversion and Biorefinery 11, 1521–1536.

Chen, B., Shan, S., Liu, J., et al., 2022a. An effective design of thermophotovoltaic metamaterial emitter for medium-temperature solar energy storage utilization. Sol. Energy 231, 194–202.

Chen, B., Shan, S., Liu, J., 2022b. A novel molten salt energy storage-solar thermophotovoltaic integrated system with mid-temperature metamaterial spectrum reshaping. Sol. Energy Mater. Sol. Cell. 243, 111799.

Collazo, J., Porteiro, J., Míguez, J.L., et al., 2012. Numerical simulation of a small-scale biomass boiler. Energy Convers. Manag. 64, 87–96.

Dan, A., Soum-Glaude, A., Carling-Plaza, A., et al., 2019. Temperature-and angle-dependent emissivity and thermal shock resistance of the W/WAlN/WAlON/Al$_2$O$_3$-based spectrally selective absorber. ACS Appl. Energy Mater. 2 (8), 5557–5567.

Durante, A., Pena-Vergara, G., Curto-Risso, P.L., et al., 2017. Thermodynamic simulation of a multi-step externally fired gas turbine powered by biomass. Energy Convers. Manag. 140, 182–191.

Gholamalizadeh, E., Chung, J.D., 2017. Exergy analysis of a pilot parabolic solar dish-Stirling system. Entropy 19 (10), 509.

Kang, X., Veeraragavan, A., 2017. Experimental demonstration of a novel approach to increase power conversion potential of a hydrocarbon fuelled, portable, thermophotovoltaic system. Energy Convers. Manag. 133, 127–137.

Karapekmez, A., Dincer, I., 2020. Comparative efficiency and environmental impact assessments of a solar-assisted combined cycle with various fuels. Appl. Therm. Eng. 164, 114409.

LaPotin, A., Schulte, K.L., Steiner, M.A., et al., 2022. Thermophotovoltaic efficiency of 40. Nature 604 (7905), 287–291.

Lenert, A., Bierman, D.M., Nam, Y., et al., 2014. A nanophotonic solar thermophotovoltaic device. Nat. Nanotechnol. 9 (2), 126–130.

Li, J., Chou, S.K., Li, Z.W., et al., 2009. A potential heat source for the micro-thermophotovoltaic (TPV) system. Chem. Eng. Sci. 64 (14), 3282–3289.

Li, P., Liu, B., Ni, Y., et al., 2015. Large-scale nanophotonic solar selective absorbers for high-efficiency solar thermal energy conversion. Adv. Mater. 27 (31), 4585–4591.

Mustafa, K.F., Abdullah, S., Abdullah, M.Z., et al., 2015. Experimental analysis of a porous burner operating on kerosene–vegetable cooking oil blends for thermophotovoltaic power generation. Energy Convers. Manag. 96, 544–560.

Mustafa, K.F., Abdullah, S., Abdullah, M.Z., et al., 2016. Comparative assessment of a porous burner using vegetable cooking oil-kerosene fuel blends for thermoelectric and thermophotovoltaic power generation. Fuel 180, 137–147.

Nam, Y., Yeng, Y.X., Lenert, A., et al., 2014. Solar thermophotovoltaic energy conversion systems with two-dimensional tantalum photonic crystal absorbers and emitters. Sol. Energy Mater. Sol. Cell. 122, 287–296.

Ni, Q., McBurney, R., Alshehri, H., et al., 2019. Theoretical analysis of solar thermophotovoltaic energy conversion with selective metafilm and cavity reflector. Sol. Energy 191, 623–628.

Peng, Q., Yang, W., Jiaqiang, E., et al., 2020. Investigation on premixed H2/C3H8/air combustion in porous medium combustor for the micro thermophotovoltaic application. Appl. Energy 260, 114352.

Qiu, K., Hayden, A.C.S., Mauk, M.G., et al., 2006. Generation of electricity using InGaAsSb and GaSb TPV cells in combustion-driven radiant sources. Sol. Energy Mater. Sol. Cells 90 (1), 68–81.

Quero, M., Korzynietz, R., Ebert, M., et al., 2014. Solugas-Operation experience of the first solar hybrid gas turbine system at MW scale. Energy Proc. 49, 1820–1830.

Rephaeli, E., Fan, S., 2009. Absorber and emitter for solar thermo-photovoltaic systems to achieve efficiency exceeding the Shockley-Queisser limit. Opt Express 17 (17), 15145–15159.

Rinnerbauer, V., Lenert, A., Bierman, D.M., et al., 2014. Metallic photonic crystal absorber emitter for efficient spectral control in high-temperature solar thermophotovoltaics. Adv. Energy Mater. 4 (12), 1400334.

Rong, L., Yuan, Z., Liu, Z., et al., 1997. Principle of Power Station Boiler. Zhejiang University Press, Hangzhou (In Chinese).

Seyf, H.R., Henry, A., 2016. Thermophotovoltaics: a potential pathway to high efficiency concentrated solar power. Energy Environ. Sci. 9 (8), 2654–2665.

Shan, S., Zhou, Z., Chen, L., et al., 2017. New weighted-sum-of-gray-gases model for typical pressurized oxy-fuel conditions. Int. J. Energy Res. 41 (15), 2576–2595.

Shan, S., Qian, B., Zhou, Z., et al., 2018. New pressurized WSGG model and the effect of pressure on the radiation heat transfer of H_2O/CO_2 gas mixtures. Int. J. Heat Mass Tran. 121, 999–1010.

Shan, S., Zhou, Z., Cen, K., 2019a. An innovative integrated system concept between oxy-fuel thermo-photovoltaic device and a Brayton-Rankine combined cycle and its preliminary thermodynamic analysis. Energy Convers. Manag. 180, 1139–1152.

Shan, S., Zhou, Z., Wang, Z., et al., 2019b. New oxy-fuel cascade thermo-photovoltaic energy conversion system: effect of cascade design and oxygen ratio. Energy Convers. Manag. 196, 1208–1221.

Shan, S., Zhou, Z., Wang, Z., et al., 2020a. A novel flame energy grading conversion system: preliminary experiment and thermodynamic parametric analysis. Int. J. Energy Res. 44 (3), 2084–2099.

Shan, S., Chen, C., Loutzenhiser, P.G., et al., 2020b. Spectral emittance measurements of micro/nanostructures in energy conversion: a review. Front. Energy 14 (3), 482–509.

Shan, S., Tian, J., Chen, B., et al., 2022a. Comparison between spectrum-split conversion and thermophotovoltaic for solar energy utilization: thermodynamic limitation and parametric analysis. Energy Convers. Manag. 255, 115331.

Shan, S., Zhang, Q., Chen, B., et al., 2022b. Effect evaluation of micro/nano structured materials on the performance of solar thermophotovoltaic system: an analysis based on measurement data. Sol. Energy 231, 1037–1047.

Shoaei, E., 2016. Performance assessment of thermophotovoltaic application in steel industry. Sol. Energy Mater. Sol. Cell. 157, 55–64.

Su, S., Lu, H., Zhang, L., et al., 2017. Solar energy utilization patterns for different district typologies using multi-objective optimization: a comparative study in China. Sol. Energy 155, 246–258.

Su, B., Han, W., Chen, Y., et al., 2018. Performance optimization of a solar assisted CCHP based on biogas reforming. Energy Convers. Manag. 171, 604–617.

Turns, S.R., 2011. An Introduction to Combustion: Concept and Application, 3th ed. McGraw-Hill, NewYork.

Ungaro, C., Gray, S.K., Gupta, M.C., 2015. Solar thermophotovoltaic system using nanostructures. Opt Express 23 (19), A1149–A1156.

Zhang, Y., Li, Q., Zhou, H., 2016. Theory and Calculation of Heat Transfer in Furnaces. Elsevier.